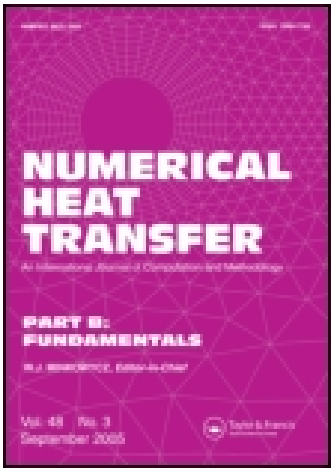

Numerical Heat Transfer, Part B: Fundamentals: An International Journal of Computation and Methodology
Publication details, including instructions for authors and subscription information:
http://www.tandfonline.com/loi/unhb20

A Compressible Thermal Lattice Boltzmann Model with Factorization Symmetry

Yongliang Feng [a] & Wen-Quan Tao [a]
[a] Key Laboratory of Thermo-Fluid Science and Engineering of MOE, School of Energy & Power Engineering, Xi'an Jiaotong University, Xian, People's Republic of China
Published online: 23 Oct 2014.

To cite this article: Yongliang Feng & Wen-Quan Tao (2014) A Compressible Thermal Lattice Boltzmann Model with Factorization Symmetry, Numerical Heat Transfer, Part B: Fundamentals: An International Journal of Computation and Methodology, 66:6, 544-562, DOI: 10.1080/10407790.2014.915679

To link to this article: http://dx.doi.org/10.1080/10407790.2014.915679

Numerical Heat Transfer, Part B, 66: 544–562, 2014

ISSN: 1040-7790 print/1521-0626 online
DOI: 10.1080/10407790.2014.915679

Taylor & Francis
Taylor & Francis Group

A COMPRESSIBLE THERMAL LATTICE BOLTZMANN MODEL WITH FACTORIZATION SYMMETRY

Yongliang Feng and Wen-Quan Tao
Key Laboratory of Thermo-Fuid Science and Engineering of MOE, School of Energy & Power Engineering, Xi'an Jiaotong University, Xian, People's Republic of China

A fully compressible multispeed lattice Boltzmann model is introduced and numerically demonstrated to simulate compressible thermal flow. The equilibrium distribution functions are derived by a nonperturbative algebraic theory in coordinate symmetry product form to avoid complex polynomial expansion of the Maxwellian function and Gauss-Hermite quadrature. An important characteristic of the proposed model is that it can be easily extendied to a multidimentional model with factorization symmetry. For compressible flows, Sod shock tube, Couette flow, and high-Mach double-reflection compressible flow are carried out to validate the present model for compressible flow and heat transfer. Numerical results are in excellent agreement with the theoretical solutions of fluid flows.

INTRODUCTION

During the past two decades, the lattice Boltzmann method (LBM) has attracted much attention and interest of researchers. There has been rapid progress in developing new models and applications in many fields [1–5]. The LBM has achieved great success in simulating nearly incompressible and isothermal fluid flows, and there has also been an ongoing effort in the construction of stable thermal compressible lattice Boltzmann equation models in order to simulate heat transfer and compressible flow. However, it has not been able to handle realistic thermal compressible flows with enough satisfaction in continuum and slip flow regimes [6, 7].

In general, the present thermal lattice Boltzmann models can be classified into three categories: the multispeed approach, the double-population approach, and the finite-difference or finite-volume hybrid approach. The multispeed approach [2, 8, 9], a straightforward extension of the athermal lattice Boltzmann model, is developed to simulate thermal compressible flows with only the velocity distribution function. The multispeed approach is based directly on gas kinetic theory, in which the hydrodynamic variables density, velocity, and internal energy (or temperature) are coupled in physical space. Recently, a lattice Boltzmann model has been extended based on the entropic LBM theory to simulate thermal and compressible flows on standard

Received 24 January 2014; accepted 7 March 2014.

Address correspondence to Wen-Quan Tao, Key Laboratory of Thermo-Fluid Science and Engineering of MOE, School of Energy and Power Engineering, Xi'an Jiaotong University, 28 Xi'an Ning Road, Xi'an, Shannxi 710049, People's Republic of China. E-mail: wqtao@mail.xjtu.edu.cn

lattices with multispeed additional terms [10–12]. The double-distribution-function thermal models [13, 14] are proposed for studying thermohydrodynamics in the incompressible limit. In these models, an internal energy density or temperature distribution function is used to simulate the temperature field. In addition, a hybrid thermal lattice Boltzmann model is proposed in which the LBM is used to solve the fluid velocity field and finite difference method for the temperature field [7, 15].

In microscopic flows, it is important to consider gaseous compressible effect and heat transfer. Lack of energy conservation in isothermal lattice Boltzmann models leads to spurious bulk viscosity and limits their use in microflows [10]. The LBM has also been developed to solve microflow problems [16, 17], due to its kinetic nature. In contrast to the direct-simulation Monte Carlo (DSMC) method, the LBM is free from statistical scatter. Furthermore, the method is definitely superior to the DSMC method for subsonic flow simulation [18]. Researchers have devoted significant efforts to extend the capability of lattice Boltzmann models for rarefied gas flows [19–23].

The setup of discrete velocity and determination of the equilibrium distribution function are two key issues for construction of a new lattice Boltzmann model. It is usually a simplified polynomial which can be derived by applying the truncated Taylor series expansion to the exponential form of the Maxwellian function in terms of the Mach number. The second-order polynomial in terms of particle speed and flow velocity is used in the common isothermal models [1]. Higher-order velocity terms must be included for compressible models [2, 9]. A theoretical framework was presented for representing hydrodynamic systems through a systematic discretization of the Boltzmann kinetic equation by means of Hermite tensor expansion of the Maxwellian function [24]. In [25], an alternative LBM was proposed to construct equilibrium distribution functions for inviscid compressible flows at high Mach number, and the conventional Maxwellian distribution function was replaced by a circular function. A high-order lattice Boltzmann model was developed to model nonequilibrium flows to capture flow characteristics in the Knudsen-layer fluid flow [21, 22]. A class of lattice equilibrium function was constructed using the maximum entropy principle [26]. Recently, an algebraic and nonperturbative theory of higher-order lattice Boltzmann models has been developed based on the symmetry of a product and maximum entropy principle [27, 28], but the model is limited to incompressible flows.

In addition, it should be pointed out that most of the previous compressible lattice Boltzmann models were proposed based on polynomial expansions of the Maxwellian or Gauss-Hermite quadrature. Consequently, the equilibrium distribution functions of those models are very complex and closely dependent on the coordinates. Furthermore, convergence of Hermite quadrature is limited by compressible condition.

In this article, a compressible thermal lattice Boltzmann model is proposed based on the symmetry of a product [27, 28]. We apply the moment relations to derive the particle equilibrium distribution functions. First, a one-dimensional model is proposed, then it is extended to a two-dimensional model based on the symmetry of a product. For the purpose of obtaining adjustable specific heat ratio and Prandtl number, a double-distribution function (DDF) compressible model is developed. We calculate a shock tube problem and Couette flow in a channel using only the

velocity distribution function and a double Mach reflection problem by DDF to examine the accuracy of the results to confirm the feasibility and validity of the present model.

COMPRESSIBLE LATTICE BOLTZMANN MODEL

The lattice Boltzmann method approximates the continuous Boltzmann equation with discretization of physical space and velocity space. Physical space is filled with a regular lattice and velocity space is discrete on a set of velocity vectors [1]. On every lattice node x, $f_i(x, t)$ indicates the density distribution of a particle with velocity e_i. We use the single time relaxation process to replace the collision term in this study. The time evolution of distribution function f_i satisfies the following equation:

$$f_i(\boldsymbol{x} + \boldsymbol{e}_i\delta_t, t + \delta_t) = f_i(\boldsymbol{x}, t) + \frac{1}{\tau}[f_i^{\mathrm{eq}}(\boldsymbol{x}, t) - f_i(\boldsymbol{x}, t)] \tag{1}$$

where τ is the relaxation parameter, δ_t is the time increment, and f_i^{eq} is the equilibrium distribution function.

Here, we intend to derive the equilibrium distribution function of the multispeed lattice Boltzmann model. First, a model in one spatial dimension is constructed. The one-dimensional Maxwell distribution function is

$$f^{\mathrm{eq}} = \rho \frac{1}{(2\pi RT)^{1/2}} \exp\left[-\frac{(\xi - u)^2}{2RT}\right] \tag{2}$$

The first five moments of the Maxwellian are listed as follows [26]:

$$M_{(0)}^M = \int f^{\mathrm{eq}} = \rho \tag{3}$$

$$M_{(1)}^M = \int f^{\mathrm{eq}}\xi = \rho u \tag{4}$$

$$M_{(2)}^M = \int f^{\mathrm{eq}}\xi^2 = \rho u^2 + \rho RT \tag{5}$$

$$M_{(3)}^M = \int f^{\mathrm{eq}}\xi^3 = \rho u^3 + 3\rho RTu \tag{6}$$

$$M_{(4)}^M = \int f^{\mathrm{eq}}\xi^4 = \rho u^4 + 6\rho RTu^2 + 3R^2T^2 \tag{7}$$

Let characteristic speed $c = \sqrt{RT_0}$ (T_0 is the characteristic temperature). A D1Q5 lattice with velocities $e_i = c(0, 1, 1, 2, 2)$ is chosen and then the equilibrium

distribution can be derived directly from the moment equations.

$$g_0^{\mathrm{eq}} = \frac{\rho}{4R^2T_0^2}\left[3R^2T^2 + 6RTu^2 + u^4 - 5R(RT + u^2)T_0 + 4R^2T_0^2\right] \tag{8}$$

$$g_1^{\mathrm{eq}} = -\frac{\rho}{6R^2T_0^2}\left\{3R^2T^2 + u^3(u + \sqrt{RT_0}) + 3RTu(2u + \sqrt{RT_0}) - 4RT_0\left[RT + u(u + \sqrt{RT_0})\right]\right\} \tag{9}$$

$$g_2^{\mathrm{eq}} = \frac{\rho}{6R^2T_0^2}\left\{-3R^2T^2 + u^3(-u + \sqrt{RT_0}) + 3RTu(-2u + \sqrt{RT_0}) + 4RT_0\left[RT + u(u - \sqrt{RT_0})\right]\right\} \tag{10}$$

$$g_3^{\mathrm{eq}} = \frac{\rho}{24R^2T_0^2}\left\{3R^2T^2 + 6RTu(u + \sqrt{RT_0}) + u^3(u + 2\sqrt{RT_0}) - RT_0\left[RT + u(u + 2\sqrt{RT_0})\right]\right\} \tag{11}$$

$$g_4^{\mathrm{eq}} = \frac{\rho}{24R^2T_0^2}\left\{3R^2T^2 + 6RTu(u - \sqrt{RT_0}) + u^3(u - 2\sqrt{RT_0}) - RT_0\left[RT + u(u - 2\sqrt{RT_0})\right]\right\} \tag{12}$$

In the above equations, g_i^{eq} is the equilibrium distribution function for one dimension. It should be noted that in the above equations the equilibrium $g_{2,4}^{\mathrm{eq}}(u, T) = g_{1,3}^{\mathrm{eq}}(-u, T)$ and the fourth-order velocity terms are included. These characteristics and higher nonlinear terms can help to improve Galilean invariance of the system. Letting $\theta = \frac{T}{T_0}$ and $v = \frac{u}{RT_0}$, we can simplify the equilibrium distribution function of one dimension as follows:

$$g_0^{\mathrm{eq}} = \frac{\rho}{4}\left[4 + v^4 - 5\theta + 3\theta^2 + v^2(-5 + 6\theta)\right] \tag{13}$$

$$g_1^{\mathrm{eq}} = -\frac{\rho}{6}\left[v^3 + v^4 + v(-4 + 3\theta) + \theta(-4 + 3\theta) + v^2(-4 + 6\theta)\right] \tag{14}$$

$$g_2^{\mathrm{eq}} = -\frac{\rho}{6}\left[-v^3 + v^4 + v(4 - 3\theta) + \theta(-4 + 3\theta) + v^2(-4 + 6\theta)\right] \tag{15}$$

$$g_3^{\mathrm{eq}} = \frac{\rho}{24}\left[2v^3 + v^4 + \theta(-1 + 3\theta) + v(-2 + 6\theta) + v^2(-1 + 6\theta)\right] \tag{16}$$

$$g_4^{\mathrm{eq}} = \frac{\rho}{24}\left[-2v^3 + v^4 + \theta(-1 + 3\theta) + v(2 - 6\theta) + v^2(-1 + 6\theta)\right] \tag{17}$$

So far, the one-dimensional lattice Boltzmann model is constructed, which includes the equilibrium distribution function, D1Q5 lattice, and evolution equation Eq. (1).

As previously indicated, the two-or three-dimensional model can be derived from the one-dimensional one by a theory based on the symmetry of a product. Taking the two-dimensional model as example, the discrete velocities can be obtained as ordered pairs $\forall e_i, e_j \in \{0, c, -c, 2c, -2c\}$. Accordingly, the two-dimensional lattice can be described with (i, j), which consists of 25 velocities, as shown in Figure 1. The two-dimensional equilibrium distribution function can be given as [27]

$$f_{(i,j)}^{\mathrm{eq}} = \rho\psi_i^{\mathrm{eq}}(v_x, \theta)\psi_j^{\mathrm{eq}}(v_y, \theta) \tag{18}$$

where the ψ_i^{eq} are known from the one-dimensional distribution function g_i^{eq} scaled by ρ. The transmission of one-dimensional information to two dimensions is completed by this simple algebraic operation. The features of the one-dimensional model are inherited by the two-dimensional one. The two-dimensional D2Q25 equilibrium distribution functions are given in Appendix A. The velocity moments of equilibrium density distribution function are calculated as follows:

$$\sum f_i^{\mathrm{eq}} = \rho \tag{19}$$

$$\sum f_i^{\mathrm{eq}} c_{i\alpha} = \rho u_\alpha \tag{20}$$

$$\sum f_i^{\mathrm{eq}} c_i^2 = \rho E \tag{21}$$

$$\sum f_i^{\mathrm{eq}} c_{i\alpha} c_{i\beta} = \rho u_\alpha u_\beta + p\delta_{\alpha\beta} \tag{22}$$

$$\sum f_i^{\mathrm{eq}} c_i^2 c_{i\alpha} = (\rho E + p) u_\alpha \tag{23}$$

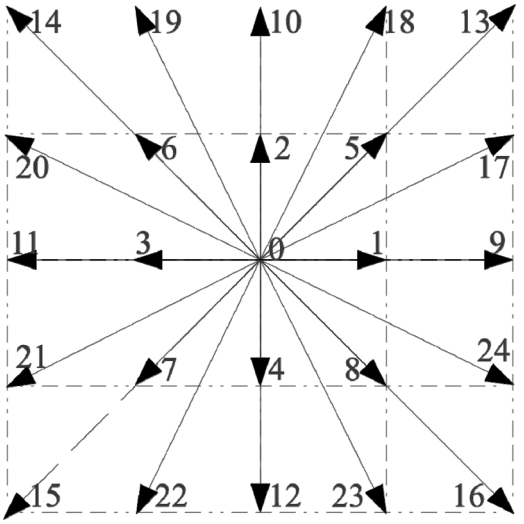

Figure 1. Setup of the discrete velocities for D2Q25 lattice.

$$\sum f_i^{\mathrm{eq}} c_{i\alpha} c_{i\beta} c_{i\gamma} = \rho u_\alpha u_\beta u_\gamma + p(u_\alpha \delta_{\beta\gamma} + u_\beta \sigma_{\gamma\alpha} + u_\gamma \sigma_{\alpha\beta}) \tag{24}$$

$$\sum f_i^{\mathrm{eq}} c_i^2 c_{i\alpha} c_{i\beta} = p(RT + E)\delta_{\alpha\beta} + (2p + \rho E) u_\alpha u_\beta \tag{25}$$

The equilibrium density distribution function satisfies the velocity moment condition to recover the macroscopic compressible Navier-Stokes equations. Using the Chapman-Enskog multiscaling technique, the distribution f_i is expanded around the equilibrium distribution $f_i^{(0)}$ as follows:

$$f_i = f_i^{(0)} + K f_i^{(1)} + K^2 f_i^{(2)} + \cdots \tag{26}$$

with

$$\sum_i f_i^{(n)} = 0 \quad \sum_i f_i \boldsymbol{c}_i^{(n)} = 0 \quad \sum_i f_i^{(n)} c_i^2 = 0 \quad n = 1, 2, \cdots \tag{27}$$

Therefore, by matching the scales of K^1, K^2, we have

$$K^1 : \left(\frac{\partial}{\partial t_1} + \boldsymbol{c}_i \cdot \nabla_1\right) f_i^{\mathrm{eq}} + \frac{f_i^{(1)}}{\tau \delta_t} = 0 \tag{28}$$

$$K^2 : \frac{\partial f_i^{\mathrm{eq}}}{\partial t_2} + \left(\frac{\partial}{\partial t_1} + \boldsymbol{c}_i \cdot \nabla_1\right)\left(1 - \frac{1}{2\tau}\right) f_i^{(1)} + \frac{f_i^{(2)}}{\tau \delta_t} = 0 \tag{29}$$

We can sum Eq. (28) and Eq. (29) over the phase space. Then the t_1, t_2 order of the continuity equation and momentum equation can be derived as

$$\frac{\partial \rho}{\partial t_1} + \nabla_1 \cdot (\rho \boldsymbol{u}) = 0 \tag{30}$$

$$\frac{\partial \rho}{\partial t_2} = 0 \tag{31}$$

$$\frac{\partial}{\partial t_1}(\rho u_\alpha) + \frac{\partial}{\partial x_{1\beta}}(\rho u_\alpha u_\beta + p\delta_{\alpha\beta}) = 0 \tag{32}$$

$$\frac{\partial}{\partial t_2}(\rho u_\alpha) + \frac{\partial}{\partial x_{1\beta}}\left(1 - \frac{1}{2\tau}\right)\left(\sum_i c_{i\alpha} c_{i\beta} f_i^{(1)}\right) = 0 \tag{33}$$

We can get the energy conservation equation by Eq. (28) and Eq. (29):

$$\frac{\partial(\rho E)}{\partial t_1} + \frac{\partial}{\partial x_{1\alpha}}[(\rho E + p) u_\alpha] = 0 \tag{34}$$

$$\frac{\partial(\rho E)}{\partial t_2} + \frac{\partial}{\partial x_{1\alpha}}\left(1 - \frac{1}{2\tau}\right)\left(\sum_i \frac{1}{2} c_{i\alpha} c_i^2 f_i^{(1)}\right) = 0 \tag{35}$$

Rewite $f_i^{(1)}$ using Eq. (29):

$$\sum_i c_{i\alpha}c_{i\beta}f_i^{(1)} = -\tau\sum_i c_{i\alpha}c_{i\beta}\left(\frac{\partial}{\partial t_1}+\boldsymbol{c}_i\cdot\nabla_1\right)f_i^{\mathrm{eq}}$$
$$= -\tau\left[\frac{\partial}{\partial t_1}\left(\rho u_\alpha u_\beta + p\delta_{\alpha\beta}\right)+\frac{\partial}{\partial x_{1\gamma}}\left(\sum f_i^{\mathrm{eq}}c_{i\alpha}c_{i\beta}c_{i\gamma}\right)\right] \tag{36}$$

$$\sum_i \frac{1}{2}c_{i\alpha}c_i^2 f_i^{(1)} = -\tau\sum_i \frac{1}{2}c_{i\alpha}c_i^2\left(\frac{\partial}{\partial t_1}+\boldsymbol{c}_i\cdot\nabla_1\right)f_i^{\mathrm{eq}}$$
$$= -\tau\frac{\partial}{\partial t_1}[(\rho E+p)u_\alpha]+\frac{\partial}{\partial x_{1\beta}}\left(\sum_i\frac{1}{2}c_i^2c_{i\alpha}c_{i\beta}f_i^{\mathrm{eq}}\right) \tag{37}$$

Using Eq. (24) and Eq. (25), we can simplify Eq. (33) and Eq. (35) as follows:

$$\frac{\partial}{\partial t_2}(\rho u_\alpha)-\frac{\partial}{\partial x_{1\beta}}\left(\tau-\frac{1}{2}\right)p\left[\left(\frac{\partial u_\alpha}{\partial x_{1\beta}}+\frac{\partial u_\beta}{\partial x_{1\alpha}}\right)-\frac{2}{D}\frac{\partial u_\gamma}{\partial x_{1\gamma}}\delta_{\alpha\beta}\right]=0 \tag{38}$$

$$\frac{\partial(\rho E)}{\partial t2}-\frac{\partial}{\partial x_{1\alpha}}\left(\tau-\frac{1}{2}\right)p\left\{u_\beta\left[\left(\frac{\partial u_\alpha}{\partial x_{1\beta}}+\frac{\partial u_\beta}{\partial x_{1\alpha}}\right)-\frac{2}{D}\frac{\partial u_\gamma}{\partial x_{1\gamma}}\delta_{\alpha\beta}\right]\right.$$
$$\left.+p(c_v+R)\frac{\partial T}{\partial x_{1\alpha}}\right\}=0 \tag{39}$$

According to Eqs. (30–32), (34), and (38) and (39), we can obtain the two-dimensional compressible Navier-Stokes equations and energy conservation equation at the second order of approximation:

$$\frac{\partial\rho}{\partial t}+\nabla\cdot(\rho\boldsymbol{u})=0 \tag{40}$$

$$\frac{\partial\rho\boldsymbol{u}}{\partial t}+\nabla\cdot(\rho\boldsymbol{u}\boldsymbol{u})=-\nabla p+\nabla\cdot\Pi \tag{41}$$

$$\frac{\partial\rho E}{\partial t}+\nabla\cdot[(\rho E+p)\boldsymbol{u}]=\nabla\cdot(\lambda\nabla T)+\nabla\cdot(\boldsymbol{u}\cdot\Pi) \tag{42}$$

where the viscous stress tensor Π is given by

$$\Pi=\mu\left[\nabla\boldsymbol{u}+(\nabla\boldsymbol{u})^T-\frac{2}{D}(\nabla\cdot\boldsymbol{u})\boldsymbol{I}\right] \tag{43}$$

where I is the unit tensor.

The dynamic viscosity and thermal conductivity are defined as

$$\mu=\left(\tau-\frac{1}{2}\right)p \tag{44}$$

$$\lambda = 2\left(\tau - \frac{1}{2}\right)p \tag{45}$$

Note that the Prandtl number of the present two-dimensional model is $\mathrm{Pr} = \mu c_p/\lambda$, where $c_p = 2$ is the specific heat at constant pressure, and the specific heat at constant volume $c_v = 1$. There are several existing methods which can be used to change specific heat ratio and Prandtl number, such as the double-distribution function, multiple-relaxation-time LBM. For the purpose of obtaining adjustable specific heat ratio and Prandtl number, the double-distribution function (DDF) method proposed by He et al. [13], Guo et al. [14], and Li et al. [29] is adopted in this article. A total energy distribution function h is introduced in the present DDF method, and its evolution equation is given as follows:

$$\begin{aligned} h_i(\boldsymbol{x}, t+\delta t) - h_i(\boldsymbol{x}, t) = &-\frac{1}{\tau}\left[h_i(\boldsymbol{x}, t) - h_i^{\mathrm{eq}}(\boldsymbol{x}, t)\right] \\ &-\frac{1}{\tau_h}\left(\boldsymbol{e}_i\boldsymbol{u} - \frac{u^2}{2}\right)\left[f_i(\boldsymbol{x}, t) - f_i^{\mathrm{eq}}(\boldsymbol{x}, t)\right] \end{aligned} \tag{46}$$

where the equilibrium total energy distribution function is given by

$$h^{\mathrm{eq}} = \frac{\xi^2 + (b-D)RT}{2} f^{\mathrm{eq}} \tag{47}$$

The total energy equilibrium distribution functions h^{eq} of the D1Q5 lattice with velocities $e_i = (0,\ c,\ c,\ 2c,\ 2c)$ are given as follows:

$$h_0^{\mathrm{eq}} = \frac{\rho(b-1)RT}{8}\left[4 + v^4 - 5\theta + 3\theta^2 + v^2(-5 + 6\theta)\right] \tag{48}$$

$$h_1^{\mathrm{eq}} = -\frac{\rho[c^2 + (b-1)RT]}{12}\left[v^3 + v^4 + v(-4 + 3\theta) + \theta(-4 + 3\theta) + v^2(-4 + 6\theta)\right] \tag{49}$$

$$h_2^{\mathrm{eq}} = -\frac{\rho[c^2 + (b-1)RT]}{12}\left[-v^3 + v^4 + v(4 - 3\theta) + \theta(-4 + 3\theta) + v^2(-4 + 6\theta)\right] \tag{50}$$

$$h_3^{\mathrm{eq}} = \frac{\rho[4c^2 + (b-1)RT]}{48}\left[2v^3 + v^4 + \theta(-1 + 3\theta) + v(-2 + 6\theta) + v^2(-1 + 6\theta)\right] \tag{51}$$

$$h_4^{\mathrm{eq}} = \frac{\rho[4c^2 + (b-1)RT]}{48}\left[-2v^3 + v^4 + \theta(-1 + 3\theta) + v(2 - 6\theta) + v^2(-1 + 6\theta)\right] \tag{52}$$

The two-dimensional total energy equilibrium distribution functions are given in Appendix B. The equilibrium total energy distribution function satisfies the following condition to recover the macroscopic compressible Navier-Stokes equations:

$$\sum h_i^{\mathrm{eq}} = \rho E \tag{53}$$

$$\sum h_i^{\mathrm{eq}} c_{i\alpha} = (\rho E + p)u_\alpha \tag{54}$$

$$\sum h_i^{\mathrm{eq}} c_i^2 = (\rho E + 2p)u^2 + p(E + T) \tag{55}$$

NUMERICAL TESTS AND RESULTS

In this section, several numerical simulations including Sod shock tube, Couette flow, and a double Mach reflection problem are carried out to verify the present model in compressible thermal flow. The Sod shock tube and Couette flow are solved by a single density distribution function. The double Mach reflection problem is tested by the DDF model including the total energy distribution function.

Sod Shock Tube

First, a standard test case of compressible flow, i.e., the shock tube problem, is simulated on grids of $1{,}024 \times 32$. The flow of the Riemann problem includes a shock wave, a contact surface, and an expansion wave; hence, it is a wonderful model problem by which the performance of the proposed numerical scheme in simulation of compressible flows can be examined [29]. The Sod shock tube test is considered with initial condition as follows:

$$\begin{aligned} \left(\frac{\rho}{\rho_0}, \frac{u}{u_0}, \frac{p}{p_0}\right) &= (1, 0, 1), 0 < \frac{x}{L} < \frac{1}{2} \\ \left(\frac{\rho}{\rho_0}, \frac{u}{u_0}, \frac{p}{p_0}\right) &= (0.125, 0, 0.1), \frac{1}{2} < \frac{x}{L} < 1 \end{aligned} \tag{56}$$

The periodical condition is taken in the y direction, and $f_i = f_i^{\mathrm{eq}}$ is set in the x direction. The specific heat ratio is 2.0 and the Prandtl number is 1.0. No discontinuity-capturing scheme is used in our present model. A typical situation of simulated results is shown in Figure 2. In the figure the profiles of the density, velocity, pressure, and temperature for the Sod shock tube obtained from the present simulation are presented by dashed lines. The theoretical solutions are represented with solid lines for comparison. The numerical results are found to be in an excellent agreement with the theoretical ones. It is noted that the discontinuities are captured exactly.

Couette Flow

Couette flow between two parallel plates is considered to valid whether the present model can describe viscous heat dissipation. A sketch of the Couette flow is shown in Figure 3. The top plate, which is H apart from the bottom plate at temperature T_1, moves with a constant velocity U. The grid of 64×64 is employed. The bottom plate at temperature T_0 is at rest. Constant viscosity and thermal conductivity are assumed. The analytical distribution of temperature in a steady state is given as

$$\begin{aligned} T_0 = T_1 &: T - T_0 = \mathrm{Pr}\frac{U^2}{2c_p}\frac{y}{H}\left(1 - \frac{y}{H}\right) \\ T_0 \neq T_1 &: \frac{T - T_0}{T_1 - T_0} = \frac{y}{H} + \frac{\mathrm{Pr\ Ec}}{2}\frac{y}{H}\left(1 - \frac{y}{H}\right) \end{aligned} \tag{57}$$

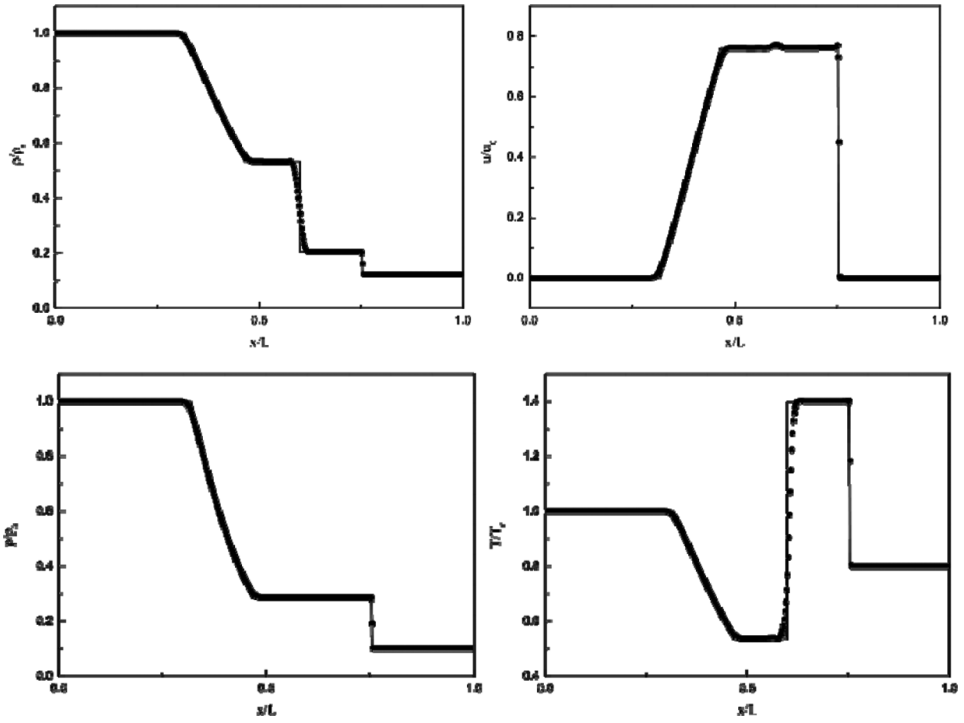

Figure 2. Comparisons between numerical and theoretical solutions of Sod shock tube.

where y is the distance from the bottom boundary, $\mathrm{Ec} = U^2/[c_p(T_1 - T_0)]$ is the Eckert number.

The viscous shear stress transmits momentum and viscous heat dissipation into the fluid. Thus, it changes the horizontal speed profile and temperature profile. Figure 4 shows simulated dimensionless temperature profiles for $U = 0.1$, $c_p = 2$, $\mathrm{Pr} = 1$, and $T_0 = T_1 = 0.4$, 0.7, 1.0, respectively. The results for all cases agree exactly with the analytical values. The distribution does not depend on plate temperature, which is also obtained from analytical solution. Figure 5 shows the simulated results for $T_1 = T_0 + 0.001$, $c_p = 2$, $\mathrm{Pr} = 1$, $U = 0.1$, 0.2, 0.3, which are in an excellent agreement

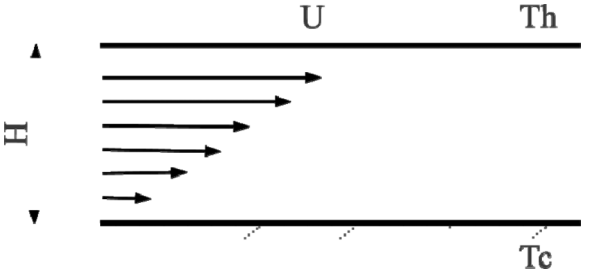

Figure 3. Sketch of Couette flow.

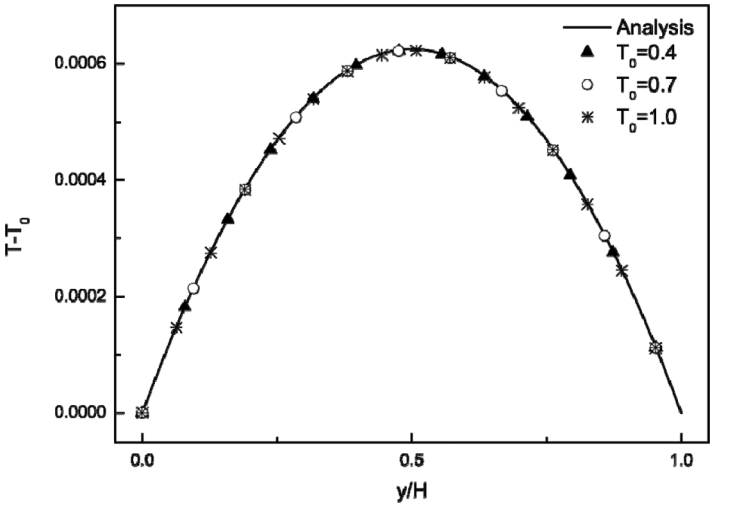

Figure 4. Temperature profiles for $U = 0.1$, $c_p = 2$, $\mathrm{Pr} = 1$, and $T_0 = T_1 = 0.4$, 0.7, 1.0.

with the analytical ones. The maximal deviations are 0.93%, 1.36%, and 1.88% for $U = 0.1$, 0.2, and 0.3, respectively.

Double Mach Reflection Problem

In the double Mach reflection problem, the computational domain is a rectangle of length = 3 and height = 1. The computational domain is divided into 360×120 grids. The case of 30° shock reflection is simulated with following conditions. The fluid in front of the shock has zero velocity, and the Mach number is 10. The inner

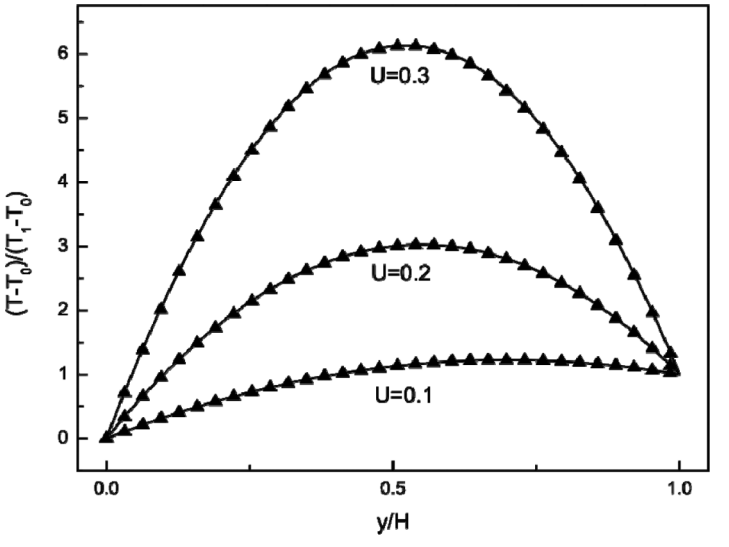

Figure 5. Temperature profiles for $T_1 = T_0 + 0.001$, $c_p = 2$, $\mathrm{Pr} = 1$, and $U = 0.1$, 0.2, 0.3.

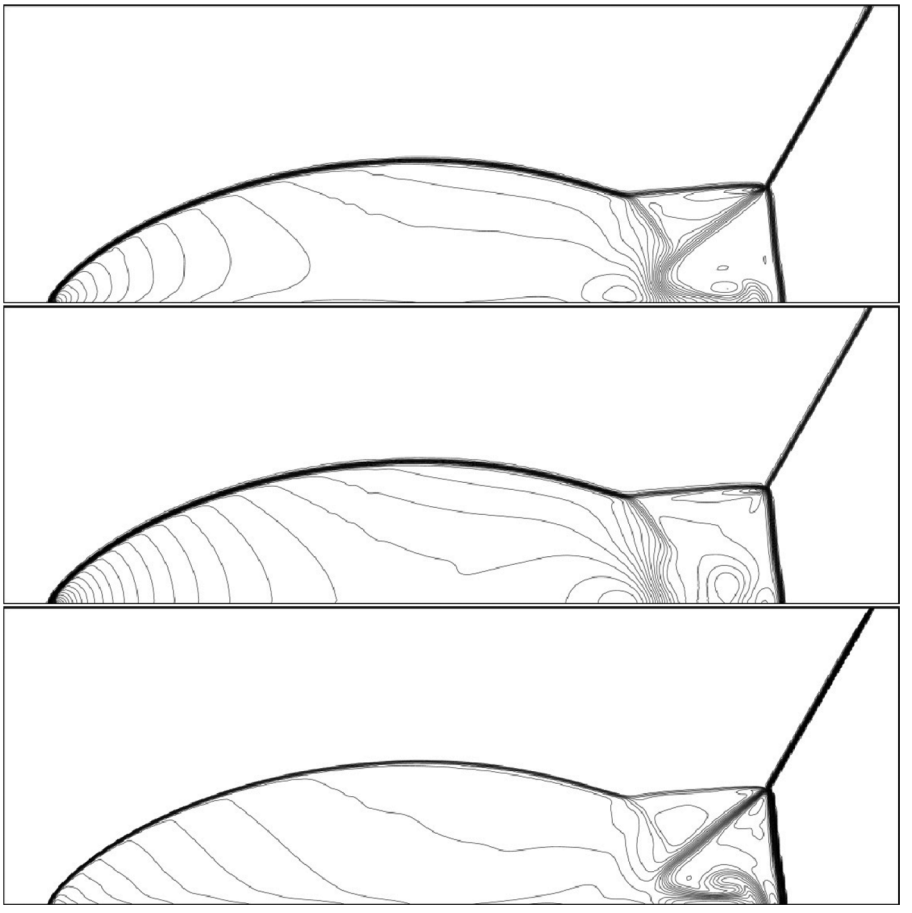

Figure 6. Density, pressure, and temperature distributions of the double Mach reflection.

x boundary is simply an "inflow" condition, in which the fluid values are set by the initial conditions in the post-shock region. The outer x boundary is a simple outflow condition, and the extrapolation technique is applied. The reflecting wall lies along the bottom of the domain. For $x \geq x_0$ this y boundary is a reflecting wall. For $x < x_0$, the lower y fluid values are set by the initial post-shock conditions. Here, we take x_0 to be $1/6$. The upper y boundary is constructed to follow the flow of the diagonal shock such that there is no interaction between the shock and this boundary. The values along the top boundary are set to describe the exact motion of the initial Mach 10 shock; it means that this test uses a time-dependent physical boundary condition at the top boundary. The initial condition is given as follows:

$$\left(\frac{\rho}{\rho_0}, \frac{u}{u_0}, \frac{v}{v_0}, \frac{p}{p_0}\right) = \left(8, 8.25 \sin\left(\frac{\pi}{3}\right), -8.25 \cos\left(\frac{\pi}{3}\right), 116.5\right), 0 < \frac{x}{L} < \frac{1}{2}$$
$$\left(\frac{\rho}{\rho_0}, \frac{u}{u_0}, \frac{v}{v_0}, \frac{p}{p_0}\right) n = (1.4, 0, 0, 1), \frac{1}{2} < \frac{x}{L} < 1 \tag{58}$$

Here, the total energy distribution function is adopted. Moreover, $b = 5$ and $R = 287$ are set in order to get $\gamma = 1.4$ and $\mathrm{Pr} = 0.71$. For capturing strong shocks of fluid flow, the fifth-order WENO scheme for space discretization and Runge-Kutta scheme in time discretization are applied in the case corresponding to the finite-difference LBM proposed by Wang et al. [30]. The flow computed by the present model is displayed in Figure 6. The results of density, pressure, and temperature distributions are shown. The complex flow features, the first Mach shock, and the second Mach shock are accurately captured. The results agree very well with those obtained using the shock-capturing scheme [31].

CONCLUSIONS

We have developed a multispeed lattice Boltzmann model for simulation of compressible thermal flow. In our model, the particle equilibrium distribution functions have been derived directly from the moment system by a simple algebraic method based on neither conventional polynomial expansions of the Maxwellian function nor Gauss-Hermite quadrature. The important point of the derivation is that the two-or three-dimensional equilibrium distribution functions are in the product form of one-dimensional equilibrium distribution functions, which are achieved by solving the one-dimensional moment system. The numerical results of the Sod shock tube and Couette flows agree well with the analytic predictions. In compressible flow with strong shock, complex flow features and Mach shock can be captured accurately using the present model. The model may be developed to be a promising tool for analyzing compressible thermal flows.

FUNDING

This work was supported by the National Science Foundation of China (51136004) and the National Program on Key Basic Research Project (973 Program, No. 2010CB227102).

REFERENCES

1. Y. H. Qian, D. D'Humires, and P. Lallemand, Lattice BGK Models for Navier-Stokes Equation, *Europhys. Lett.*, vol. 17, pp. 479–484, 1992.
2. Y. H. Qian, Smulating Thermohydrodynamics with Lattice BGK Models, *J. Sci. Comput.*, vol. 8, pp. 231–242, 1993.
3. S. Y. Chen and G. D. Doolen, Lattice Boltzmann Method for Fluid Flows, *Annu. Rev. Fluid Mech.*, vol. 30, pp. 329–364, 1998.
4. S. Succi, The Lattice Boltzamnn Equation: For Fluid Dynamics and beyond, *Numerical Mathematics and Scientific Computation*, Clarendon Press, Oxford, UK, 2001.
5. L. Jahanshaloo, E. Pouryazdanpanah, S. Che, and A. Nor, Review on the Application of the Lattice Boltzmann Method for Turbulent Flow Simulation, *Numeri. Heat Transfer A*, vol. 64, pp. 938–958, 2013.
6. P. Lopez and Y. Bayazitoglu, High Knudsen Number Thermal Flows with the D2Q13 Lattice Boltzmann Model, *Numer. Heat Transfer A*, vol. 64, pp. 93–106, 2013.
7. P. Lallemand and L. S. Luo, Hybrid Finite-Difference Thermal Lattice Boltzmann Equation, *Int. J. Mod. Phys. B*, vol. 17, pp. 41–47, 2003.

8. F. J. Alexander, H. Chen, S. Chen, and G. D. Doolen, Lattice Boltzmann Model for Compressible Fluids, *Phys. Rev. A*, vol. 46, pp. 1967–1970, 1992.
9. Y. Chen, H. Ohashi, and M. Akiyama, Thermal Lattice Bhatnagar-Gross-Krook Model without Nonlinear Deviations in Macrodynamic Equations, *Phys. Rev. E*, vol. 50, pp. 2776–2783, 1994.
10. N. I. Prasianakis, S. S. Chikatamarla, I. V. Karlin, S. Ansumali, and K. Boulouchos, Entropic Lattice Boltzmann Method for Simulation of Thermal Flows, *Math. Comput. Simulation*, vol. 72, pp. 179–183, 2006.
11. N. I. Prasianakis and I. V. Karlin, Lattice Boltzmann Method for Thermal Flow Simulation on Standard Lattices, *Phys. Rev. E*, vol. 76, 016702, 2007.
12. N. I. Prasianakis and I. V. Karlin, Lattice Boltzmann Method for Simulation of Compressible Flows on Standard Lattices, *Phys. Rev. E*, vol. 78, 016704, 2008.
13. X. Y. He, S. Y. Chen, and G. D. Doolen, A Novel Thermal Model for the Lattice Boltzmann Method in Incompressible Limit, *J. Comput. Phys.*, vol. 146, pp. 282–300, 1998.
14. Z. L. Guo, C. G. Zheng, B. C. Shi, and T. S. Zhao, Thermal Lattice Boltzmann Equation for Low Mach Number Flows: Decoupling Model, *Phys. Rev. E*, vol. 75, 036704, 2007.
15. P. Lallemand and L. S. Luo, Theory of the Lattice Boltzmann Method: Acoustic and Thermal Properties in Two and Three Dimensions, *Phys. Rev. E*, vol. 68, 036706, 2003.
16. V. Sofonea and R. F. Sekerka, Diffuse-Reflection Boundary Conditions for a Thermal Lattice Boltzmann Model in Two Dimensions: Evidence of Temperature Jump and Slip Velocity in Microchannels, *Phys. Rev. E*, vol. 71, 066709, 2005.
17. Y. H. Zhang, X. J. Gu, R. W. Barber, and D. R. Emerson, Capturing Knudsen Layer Phenomena Using a Lattice Boltzmann Model, *Phys. Rev. E*, vol. 74, 046704, 2006.
18. M. Koji, Numerical Simulation for Gas Microflows Using Boltzmann Equation, *Comput. Fluids*, vol. 35, pp. 978–985, 2006.
19. S. H. Kim, H. Pitsch, and I. D. Boyd, Accuracy of Higher-Order Lattice Boltzmann Methods for Microscale Flows with Finite Knudsen Numbers, *J. Comput. Phys.*, vol. 227, pp. 8655–8671, 2008.
20. S. Ansumali, I. V. Karlin, S. Arcidiacono, A. Abbas, and N. I. Prasianakis, Hydrodynamics beyond Navier-Stokes: Exact Solution to the Lattice Boltzmann Hierarchy, *Phys. Rev. Lett.*, vol. 98, 124502, 2007.
21. G. H. Tang, Y. H. Zhang, and D. R. Emerson, Lattice Boltzmann Models for Nonequilibrium Gas Flows, *Phys. Rev. E*, vol. 77, 046701, 2008.
22. J. P. Meng, Y. H. Zhang, and X. W. Shan, Multiscale Lattice Boltzmann Approach to Modeling Gas Flows, *Phys. Rev. E*, vol. 83, 046701, 2011.
23. Q. Li, Y. He, G. Tang, and W. Tao, Lattice Boltzmann Modeling of Microchannel Flows in the Transition Flow Regime, *Microfluid. Nanofluid.*, vol. 10, pp. 607–618, 2011.
24. X. W. Shan, X. F. Yuan, and H. D. Chen, Kinetic Theory Representation of Hydrodynamics: A Way beyond the Navier-Stokes Equation, *J. Fluid Mech.*, vol. 550, pp. 413–441, 2006.
25. K. Qu, C. Shu, and Y. T. Chew, Alternative Method to Construct Equilibrium Distribution Functions in Lattice-Boltzmann Method Simulation of Inviscid Compressible Flows at High Mach Number, *Phys. Rev. E*, vol. 75, 036706, 2007.
26. I. V. Karlin, A. N. Gorban, S. Succi, and V. Boffi, Maximum Entropy Principle for Lattice Kinetic Equations, *Phys. Rev. Lett.*, vol. 81, pp. 6–9, 1998.
27. I. Karlin and P. Asinari, Factorization Symmetry in the Lattice Boltzmann Method, *Physica A—Stat. Mech. Appl.*, vol. 389, pp. 1530–1548, 2010.
28. S. S. Chikatamarla and I. V. Karlin, Lattices for the Lattice Boltzmann Method, *Phys. Rev. E*, vol. 79, 046701, 2009.
29. Q. Li, Y. L. He, Y. Wang, and W. Q. Tao, Coupled Double-Distribution-Function Lattice Boltzmann Method for the Compressible Navier-Stokes Equations, *Phys. Rev. E*, vol. 76, 056705, 2007.

30. Y. Wang, Y. He, Q. Li, G. Tang, and W. Tao, Lattice Boltzmann Model for Simulating Viscous Compressible Flows, *Int. J. Mod. Phys. C*, vol. 21, pp. 383–407, 2010.
31. P. Woodward and P. Colella, The Numerical Simulation of Two-Dimensional Fluid Flow with Strong Shocks, *J. Comput. Phys.*, vol. 54, pp. 115–173, 1984.

APPENDIX A. TWO-DIMENSIONAL EQUILIBRIUM DISTRIBUTION FUNCTIONS

We give here the equilibrium distribution functions of the D2Q25 model. u is the dimensionless velocity in the x direction, v is dimensionless velocity in the y direction, and $\theta = T/T_0$ is dimensionless temperature.

$$f_0^{\mathrm{eq}} = \frac{\rho}{16}[4 + 3\theta^2 - 5u^2 + u^4 + \theta(-5 + 6u^2)] \\ [4 + 3\theta^2 - 5v^2 + v^4 + \theta(-5 + 6v^2)]$$

$$f_1^{\mathrm{eq}} = -\frac{\rho}{24}[3\theta^2 + \theta(-4 + 3u + 6u^2) + u(-4 - 4u + u^2 + u^3)] \\ [4 + 3\theta^2 - 5v^2 + v^4 + \theta(-5 + 6v^2)]$$

$$f_2^{\mathrm{eq}} = \frac{\rho}{24}[-3\theta^2 - \theta(-4 + 3v + 6v^2) - v(-4 - 4v + v^2 + v^3)] \\ [4 + 3\theta^2 - 5u^2 + u^4 + \theta(-5 + 6u^2)]$$

$$f_3^{\mathrm{eq}} = \frac{\rho}{24}[-3\theta^2 + \theta(4 + 3u - 6u^2) + u(-4 + 4u + u^2 - u^3)] \\ [4 + 3\theta^2 - 5v^2 + v^4 + \theta(-5 + 6v^2)]$$

$$f_4^{\mathrm{eq}} = \frac{\rho}{24}[-3\theta^2 + \theta(4 + 3v - 6v^2) + v(-4 + 4v + v^2 - v^3)] \\ [4 + 3\theta^2 - 5u^2 + u^4 + \theta(-5 + 6u^2)]$$

$$f_5^{\mathrm{eq}} = -\frac{\rho}{36}[3\theta^2 + \theta(-4 + 3u + 6u^2) + u(-4 - 4u + u^2 + u^3)] \\ [-3\theta^2 - \theta(-4 + 3v + 6v^2) - v(-4 - 4v + v^2 + v^3)]$$

$$f_6^{\mathrm{eq}} = \frac{\rho}{36}[-3\theta^2 + \theta(4 + 3u - 6u^2) + u(-4 + 4u + u^2 - u^3)] \\ [-3\theta^2 - \theta(-4 + 3v + 6v^2) - v(-4 - 4v + v^2 + v^3)]$$

$$f_7^{\mathrm{eq}} = \frac{\rho}{36}[-3\theta^2 + \theta(4 + 3u - 6u^2) + u(-4 + 4u + u^2 - u^3)] \\ [-3\theta^2 + \theta(4 + 3v - 6v^2) + v(-4 + 4v + v^2 - v^3)]$$

$$f_8^{\mathrm{eq}} = -\frac{\rho}{36}[3\theta^2 + \theta(-4 + 3u + 6u^2) + u(-4 - 4u + u^2 + u^3)] \\ [-3\theta^2 + \theta(4 + 3v - 6v^2) + v(-4 + 4v + v^2 - v^3)]$$

$$f_9^{\mathrm{eq}} = \frac{\rho}{96}[4 + 3\theta^2 - 5v^2 + v^4 + \theta(-5 + 6v^2)]$$
$$[3\theta^2 + \theta(-1 + 6u + 6u^2) + u(-2 - u + 2u^2 + u^3)]$$

$$f_{10}^{\mathrm{eq}} = \frac{\rho}{96}[4 + 3\theta^2 - 5u^2 + u^4 + \theta(-5 + 6u^2)]$$
$$[3\theta^2 + \theta(-1 + 6v + 6v^2) + v(-2 - v + 2v^2 + v^3)]$$

$$f_{11}^{\mathrm{eq}} = \frac{\rho}{96}[4 + 3\theta^2 - 5v^2 + v^4 + \theta(-5 + 6v^2)]$$
$$[3\theta^2 + \theta(-1 - 6u + 6u^2) + u(2 - u - 2u^2 + u^3)]$$

$$f_{12}^{\mathrm{eq}} = \frac{\rho}{96}[4 + 3\theta^2 - 5u^2 + u^4 + \theta(-5 + 6u^2)]$$
$$[3\theta^2 + \theta(-1 - 6v + 6v^2) + v(2 - v - 2v^2 + v^3)]$$

$$f_{13}^{\mathrm{eq}} = \frac{\rho}{576}[3\theta^2 + \theta(-1 + 6u + 6u^2) + u(-2 - u + 2u^2 + u^3)]$$
$$[3\theta^2 + \theta(-1 + 6v + 6v^2) + v(-2 - v + 2v^2 + v^3)]$$

$$f_{14}^{\mathrm{eq}} = \frac{\rho}{576}[3\theta^2 + \theta(-1 - 6u + 6u^2) + u(2 - u - 2u^2 + u^3)]$$
$$[3\theta^2 + \theta(-1 + 6v + 6v^2) + v(-2 - v + 2v^2 + v^3)]$$

$$f_{15}^{\mathrm{eq}} = \frac{\rho}{576}[3\theta^2 + \theta(-1 - 6u + 6u^2) + u(2 - u - 2u^2 + u^3)]$$
$$[3\theta^2 + \theta(-1 - 6v + 6v^2) + v(2 - v - 2v^2 + v^3)]$$

$$f_{16}^{\mathrm{eq}} = \frac{\rho}{576}[3\theta^2 + \theta(-1 + 6u + 6u^2) + u(-2 - u + 2u^2 + u^3)]$$
$$[3\theta^2 + \theta(-1 - 6v + 6v^2) + v(2 - v - 2v^2 + v^3)]$$

$$f_{17}^{\mathrm{eq}} = \frac{\rho}{144}[3\theta^2 + \theta(-1 + 6u + 6u^2) + u(-2 - u + 2u^2 + u^3)]$$
$$[-3\theta^2 - \theta(-4 + 3v + 6v^2) - v(-4 - 4v + v^2 + v^3)]$$

$$f_{18}^{\mathrm{eq}} = -\frac{\rho}{144}[3\theta^2 + \theta(-1 + 6v + 6v^2) + v(-2 - v + 2v^2 + v^3)]$$
$$[3\theta^2 + \theta(-4 + 3u + 6u^2) + u(-4 - 4u + u^2 + u^3)]$$

$$f_{19}^{\mathrm{eq}} = \frac{\rho}{144}[3\theta^2 + \theta(-1 + 6v + 6v^2) + v(-2 - v + 2v^2 + v^3)]$$
$$[-3\theta^2 + \theta(4 + 3u - 6u^2) + u(-4 + 4u + u^2 - u^3)]$$

$$f_{20}^{\mathrm{eq}} = \frac{\rho}{144}[3\theta^2 + \theta(-1 - 6u + 6u^2) + u(2 - u - 2u^2 + u^3)]$$
$$[-3\theta^2 - \theta(-4 + 3v + 6v^2) - v(-4 - 4v + v^2 + v^3)]$$

$$f_{21}^{\mathrm{eq}} = \frac{\rho}{144}[3\theta^2 + \theta(-1 - 6u + 6u^2) + u(2 - u - 2u^2 + u^3)]$$
$$[-3\theta^2 + \theta(4 + 3v - 6v^2) + v(-4 + 4v + v^2 - v^3)]$$

$$f_{22}^{\mathrm{eq}} = \frac{\rho}{144}[3\theta^2 + \theta(-1 - 6v + 6v^2) + v(2 - v - 2v^2 + v^3)]$$
$$[-3\theta^2 + \theta(4 + 3u - 6u^2) + u(-4 + 4u + u^2 - u^3)]$$

$$f_{23}^{\mathrm{eq}} = -\frac{\rho}{144}[3\theta^2 + \theta(-1 - 6v + 6v^2) + v(2 - v - 2v^2 + v^3)]$$
$$[3\theta^2 + \theta(-4 + 3u + 6u^2) + u(-4 - 4u + u^2 + u^3)]$$

$$f_{24}^{\mathrm{eq}} = \frac{\rho}{144}[3\theta^2 + \theta(-1 + 6u + 6u^2) + u(-2 - u + 2u^2 + u^3)]$$
$$[-3\theta^2 + \theta(4 + 3v - 6v^2) + v(-4 + 4v + v^2 - v^3)]$$

APPENDIX B. TWO-DIMENSIONAL TOTAL ENERGY EQUILIBRIUM DISTRIBUTION FUNCTIONS

We give here the total energy equilibrium distribution functions of the D2Q25 model. u is dimensionless velocity in the x direction, v is dimensionless velocity in the y direction, and $\theta = T/T_0$ is dimensionless temperature.

$$h_0^{\mathrm{eq}} = \frac{e_i^2 + (b-2)RT}{2}\frac{\rho}{16}[4 + 3\theta^2 - 5u^2 + u^4 + \theta(-5 + 6u^2)]$$
$$[4 + 3\theta^2 - 5v^2 + v^4 + \theta(-5 + 6v^2)]$$

$$h_1^{\mathrm{eq}} = -\frac{e_i^2 + (b-2)RT}{2}\frac{\rho}{24}[3\theta^2 + \theta(-4 + 3u + 6u^2) + u(-4 - 4u + u^2 + u^3)]$$
$$[4 + 3\theta^2 - 5v^2 + v^4 + \theta(-5 + 6v^2)]$$

$$h_2^{\mathrm{eq}} = \frac{e_i^2 + (b-2)RT}{2}\frac{\rho}{24}[-3\theta^2 - \theta(-4 + 3v + 6v^2) - v(-4 - 4v + v^2 + v^3)]$$
$$[4 + 3\theta^2 - 5u^2 + u^4 + \theta(-5 + 6u^2)]$$

$$h_3^{\mathrm{eq}} = \frac{e_i^2 + (b-2)RT}{2}\frac{\rho}{24}[-3\theta^2 + \theta(4 + 3u - 6u^2) + u(-4 + 4u + u^2 - u^3)]$$
$$[4 + 3\theta^2 - 5v^2 + v^4 + \theta(-5 + 6v^2)]$$

$$h_4^{\mathrm{eq}} = \frac{e_i^2 + (b-2)RT}{2}\frac{\rho}{24}[-3\theta^2 + \theta(4 + 3v - 6v^2) + v(-4 + 4v + v^2 - v^3)]$$
$$[4 + 3\theta^2 - 5u^2 + u^4 + \theta(-5 + 6u^2)]$$

$$h_5^{\mathrm{eq}} = -\frac{e_i^2 + (b-2)RT}{2}\frac{\rho}{36}[3\theta^2 + \theta(-4 + 3u + 6u^2) + u(-4 - 4u + u^2 + u^3)]$$
$$[-3\theta^2 - \theta(-4 + 3v + 6v^2) - v(-4 - 4v + v^2 + v^3)]$$

$$h_6^{\mathrm{eq}} = \frac{e_i^2 + (b-2)RT}{2}\frac{\rho}{36}[-3\theta^2 + \theta(4 + 3u - 6u^2) + u(-4 + 4u + u^2 - u^3)]$$
$$[-3\theta^2 - \theta(-4 + 3v + 6v^2) - v(-4 - 4v + v^2 + v^3)]$$

$$h_7^{\mathrm{eq}} = \frac{e_i^2 + (b-2)RT}{2}\frac{\rho}{36}[-3\theta^2 + \theta(4 + 3u - 6u^2) + u(-4 + 4u + u^2 - u^3)]$$
$$[-3\theta^2 + \theta(4 + 3v - 6v^2) + v(-4 + 4v + v^2 - v^3)]$$

$$h_8^{\mathrm{eq}} = -\frac{e_i^2 + (b-2)RT}{2}\frac{\rho}{36}[3\theta^2 + \theta(-4 + 3u + 6u^2) + u(-4 - 4u + u^2 + u^3)]$$
$$[-3\theta^2 + \theta(4 + 3v - 6v^2) + v(-4 + 4v + v^2 - v^3)]$$

$$h_9^{\mathrm{eq}} = \frac{e_i^2 + (b-2)RT}{2}\frac{\rho}{96}[4 + 3\theta^2 - 5v^2 + v^4 + \theta(-5 + 6v^2)]$$
$$[3\theta^2 + \theta(-1 + 6u + 6u^2) + u(-2 - u + 2u^2 + u^3)]$$

$$h_{10}^{\mathrm{eq}} = \frac{e_i^2 + (b-2)RT}{2}\frac{\rho}{96}[4 + 3\theta^2 - 5u^2 + u^4 + \theta(-5 + 6u^2)]$$
$$[3\theta^2 + \theta(-1 + 6v + 6v^2) + v(-2 - v + 2v^2 + v^3)]$$

$$h_{11}^{\mathrm{eq}} = \frac{e_i^2 + (b-2)RT}{2}\frac{\rho}{96}[4 + 3\theta^2 - 5v^2 + v^4 + \theta(-5 + 6v^2)]$$
$$[3\theta^2 + \theta(-1 - 6u + 6u^2) + u(2 - u - 2u^2 + u^3)]$$

$$h_{12}^{\mathrm{eq}} = \frac{e_i^2 + (b-2)RT}{2}\frac{\rho}{96}[4 + 3\theta^2 - 5u^2 + u^4 + \theta(-5 + 6u^2)]$$
$$[3\theta^2 + \theta(-1 - 6v + 6v^2) + v(2 - v - 2v^2 + v^3)]$$

$$h_{13}^{\mathrm{eq}} = \frac{e_i^2 + (b-2)RT}{2}\frac{\rho}{576}[3\theta^2 + \theta(-1 + 6u + 6u^2) + u(-2 - u + 2u^2 + u^3)]$$
$$[3\theta^2 + \theta(-1 + 6v + 6v^2) + v(-2 - v + 2v^2 + v^3)]$$

$$h_{14}^{\mathrm{eq}} = \frac{e_i^2 + (b-2)RT}{2}\frac{\rho}{576}[3\theta^2 + \theta(-1 - 6u + 6u^2) + u(2 - u - 2u^2 + u^3)]$$
$$[3\theta^2 + \theta(-1 + 6v + 6v^2) + v(-2 - v + 2v^2 + v^3)]$$

$$h_{15}^{\mathrm{eq}} = \frac{e_i^2 + (b-2)RT}{2}\frac{\rho}{576}[3\theta^2 + \theta(-1 - 6u + 6u^2) + u(2 - u - 2u^2 + u^3)]$$
$$[3\theta^2 + \theta(-1 - 6v + 6v^2) + v(2 - v - 2v^2 + v^3)]$$

$$h_{16}^{\mathrm{eq}} = \frac{e_i^2 + (b-2)RT}{2}\frac{\rho}{576}[3\theta^2 + \theta(-1+6u+6u^2) + u(-2-u+2u^2+u^3)]$$
$$[3\theta^2 + \theta(-1-6v+6v^2) + v(2-v-2v^2+v^3)]$$

$$h_{17}^{\mathrm{eq}} = \frac{e_i^2 + (b-2)RT}{2}\frac{\rho}{144}[3\theta^2 + \theta(-1+6u+6u^2) + u(-2-u+2u^2+u^3)]$$
$$[-3\theta^2 - \theta(-4+3v+6v^2) - v(-4-4v+v^2+v^3)]$$

$$h_{18}^{\mathrm{eq}} = -\frac{e_i^2 + (b-2)RT}{2}\frac{\rho}{144}[3\theta^2 + \theta(-1+6v+6v^2) + v(-2-v+2v^2+v^3)]$$
$$[3\theta^2 + \theta(-4+3u+6u^2) + u(-4-4u+u^2+u^3)]$$

$$h_{19}^{\mathrm{eq}} = \frac{e_i^2 + (b-2)RT}{2}\frac{\rho}{144}[3\theta^2 + \theta(-1+6v+6v^2) + v(-2-v+2v^2+v^3)]$$
$$[-3\theta^2 + \theta(4+3u-6u^2) + u(-4+4u+u^2-u^3)]$$

$$h_{20}^{\mathrm{eq}} = \frac{e_i^2 + (b-2)RT}{2}\frac{\rho}{144}[3\theta^2 + \theta(-1-6u+6u^2) + u(2-u-2u^2+u^3)]$$
$$[-3\theta^2 - \theta(-4+3v+6v^2) - v(-4-4v+v^2+v^3)]$$

$$h_{21}^{\mathrm{eq}} = \frac{e_i^2 + (b-2)RT}{2}\frac{\rho}{144}[3\theta^2 + \theta(-1-6u+6u^2) + u(2-u-2u^2+u^3)]$$
$$[-3\theta^2 + \theta(4+3v-6v^2) + v(-4+4v+v^2-v^3)]$$

$$h_{22}^{\mathrm{eq}} = \frac{e_i^2 + (b-2)RT}{2}\frac{\rho}{144}[3\theta^2 + \theta(-1-6v+6v^2) + v(2-v-2v^2+v^3)]$$
$$[-3\theta^2 + \theta(4+3u-6u^2) + u(-4+4u+u^2-u^3)]$$

$$h_{23}^{\mathrm{eq}} = -\frac{e_i^2 + (b-2)RT}{2}\frac{\rho}{144}[3\theta^2 + \theta(-1-6v+6v^2) + v(2-v-2v^2+v^3)]$$
$$[3\theta^2 + \theta(-4+3u+6u^2) + u(-4-4u+u^2+u^3)]$$

$$h_{24}^{\mathrm{eq}} = \frac{e_i^2 + (b-2)RT}{2}\frac{\rho}{144}[3\theta^2 + \theta(-1+6u+6u^2) + u(-2-u+2u^2+u^3)]$$
$$[-3\theta^2 + \theta(4+3v-6v^2) + v(-4+4v+v^2-v^3)]$$